Rendiconti Lincei 20, 1 – 19 (2009)
DOI: 10.1007/s12210-009-0001-8

Ahmed Hosny · Sherif M. El-Hady · A. Mohamed Abou El-Ela · Giuliano F. Panza · Ali Tealeb · Mahdi Adb El Rahman

Magma Intrusion in the Upper Crust of the Abu Dabbab Area, South East of Egypt from Vp and Vp/Vs Tomography

Received: 21 December 2007 / Accepted: 21 January 2008 –

Abstract 3-D images of P-wave velocity and Vp/Vs ratio have been produced for the upper crust of the Abu Dabbab area, North Mars Alam city. The inversion of local travel times of high quality data recorded at eleven mobile seimic stations around the study area is carried out. The best, in the least-squares sense, 1-D Vp model and the average value of Vp/Vs (1.72) were computed as prerequisites of the 3-D inversion that reaches a depth of 14 km. From the 3-D

A. Hosny (✉)
6 El-Marsad St., Sismology Department, National Research Institute of Astronomy and Geophysics, 11421 Helwan, Cairo, Egypt
Phone: +202 25560645 Fax: +202 25548020 E-mail: ahhosny2000@yahoo.com

S.M. El-Hady
6 El-Marsad St., Sismology Department, National Research Institute of Astronomy and Geophysics, 11421 Helwan, Cairo, Egypt
Phone: +202 25583887 Fax: +202 25548020 E-mail: shsh11s@yahoo.com

A.M. Abou El-Ela
6 El-Marsad St., Sismology Department, National Research Institute of Astronomy and Geophysics, 11421 Helwan, Cairo, Egypt
Phone: +202 25583887 Fax: +202 25548020 E-mail: abuoelela99@hotmail.com or amin@nriag.sci.eg

G.F. Panza
Via Weiss, 4 Department of Earth Science, Trieste university and the Abdus Salam ICTP/ESP section, Head of SAND Group I-34127 Trieste (Italy)
phone: +39-040-5582117 or mobile 338-8371527 Fax: +39-040-22407334 or +39-040-5582111 or +39-040-575519 E-mail: panza@dst.units.it

A. Tealeb
Seismology Department, National Research Institute of Astronomy and Geophysics, Helwan, Cairo, Egypt

M.A. El Rahman
Geophysics Department, Faculty of Science, Ain Shams University

model it is evident that the distributions of Vp and Vp/Vs are characterized by marked lateral and vertical variations delineating structural heterogeneities. Due to the presence of a thin layer of sedimentary rocks saturated with surface water, low P-wave velocity and high Vp/Vs values are noticed near the surface. At greater depths, high Vp and low Vp/Vs zones may indicate crustal rocks with relatively higher rigidity and brittle behavior, while high Vp/Vs and low Vp may identify zones of relatively softer rocks, with ductile behavior. Low P-wave velocity values are observed at the intersections among the faults. A possibility of some magma intrusion could be associated with the high Vp/Vs values which form an elongated anomaly, in the central part of the study area, which extends from a depth of 12 km to about 1-2 km of depth.

If the obtained 3-D model is used in the relocation of selected events, they turn out to be strongly clustered in correspondence with the high velocity anomalies detected in the central part of the study area. Most of the seismicity tends to occur at the boundaries between the high and low velocity anomalies and at pre-existing weakness zones, i.e. the areas of intersection among different faults. The occurrence of the seismic activity in the vicinity of low velocity anomalies and at the boundary between velocity contrast could also be explained by the occurrence of serpentinization processes in the crust of the study area.

Kewwords Seismic tomography, Vp, Vp/Vs structures, Magma intrusion

Subject codes G18009, G11004, G13007

1 Introduction

On the west bank of the Red Sea coast line, South East of Egypt, there is an active seismic area which is the Abu Dabbab area. This area is located to the north of Marsa-Alam city between longitudes 33.67° and 35.31°E and latitudes 24.55° and 25.65°N, see Fig. 1.

Seismic activity is recorded daily and earthquake swarms accompanied by sounds have been known since the beginning of the 20th century in this area (Morgan et al. 1981). After 1970, the swarms were instrumentally observed and discussed by several authors (Hamada 1968; Fairhead and Girdler 1970; Daggett and Morgan 1977; Daggett et al. 1986; Hassoup 1987; Kebeasy 1990; El-Hady 1993; Ibrahim and Yokoyama 1994). In addition to the swarms which occurred in 1976, 1984 and 1993, there have been four microearthquake swarms in January 2003, April 2003, October 2003 and August 2004. However, two recent events (12 November 1955 (M = 6.0) and 2 July 1984 (M = 5.1)) were widely felt in Upper Egypt (see, Fig. 1).

Recent seismotectonics studies on the swarm of August 2004 have been done by Hosny (2008) and Badawy et al. (2008) using moment tensor inversion

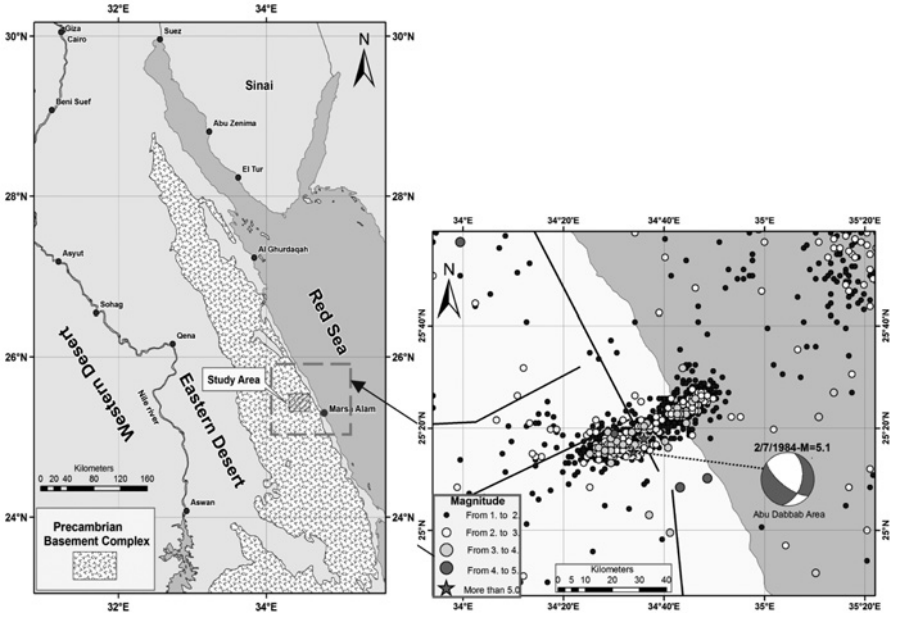

Fig. 1 Key map of the study area. The regional seismicity from (1900–2007) close to the study area has been shown in the right part of the figure (from 1900–2007). Black lines represent the major faults in the basement interpreted from magnetic intenisty maps (after Bayoumi et al. 1979). The focal mechanism solution after, Kebeasy (1990).

and focal mechanism solutions. They concluded that in the Abu Dabbab area, the distribution of microearthquakes tends to align in an ENE-WSW direction marking a zone of activity transverse to the Red Sea. The characteristics of the seismic activity at Abu Dabbab suggest that the area's seismicity is related to local sources rather than regional tectonics. Focal mechanism solutions show different fault styles. Indeed, all these fault trends are evidently caused by surface faults (Badawy et al. 2008).

Since the pioneering work of Aki and Lee (1976), a great number of researchers have used local earthquake tomography to study the three-dimensional (3-D) velocity structure of the crust and upper mantle, and great advances have been made in the theory and application of this approach during the last two decades. At present, local earthquake tomography has become a powerful tool to investigate the structural heterogeneity of the crust and upper mantle, and its relationship to seismic and volcanic activity in a region. However, there are still some limitations in local earthquake tomography. One of them is that the spatial resolution of the tomographic images obtained is generally limited by the spacing between the used seismic stations (Zhao and Laske 2005).

Local Seismic Tomography is a non-linear algorithm. The non-linearity stems from the fact that both the Earth model and the hypocentral locations

must be determined simultaneously. In most cases, the solution to the non-linear inverse problem is obtained through linearization with a reference model. Thus the procedure usually starts with the definition of an initial model (a priori model) as close as possible to reality. The choice of the initial model, necessary for the linearized inversion of travel times, is thus a crucial decision that intrinsically affects the final results.

Thurber et al. (1999) provided a suitable solution to the problem in order to determine 3-D images of the Earth. They proposed a method that uses the a priori velocity model (1-D model), travel times, and hypocentral locations. A good distribution of local earthquakes is required through the area under investigation as well as a good selection of the grid nodes where the a priori model is defined. The grid step depends on the number of rays passing through the model.

In the present study, by using good quality data, the three dimensional Vp, Vp/Vs, and Vs models are computed. In the subsequent sections a detailed description of the data and the procedure for estimating the subsurface velocity structures will be given. The procedure is subdivided into a number of steps. The first step deals with the construction of the 1-D a priori model using VELEST (Kissling et al. 1995). The other steps deal with the computations of the 3-D Vp, Vs, and Vp/Vs models.

2 Geologic and structural setting

The regional geology of the Abu Dabbab area is related essentially to the geologic setting of the Central Eastern Desert (CED), Fig. 1. The Red Sea rifting ($\sim$ 30 my ago) led to isostatic readjustment and uplift of the bordering of (CED) continental margins (Martinez and Cochran 1988). Subsequent erosion removed their Phanerozoic sedimentary cover and exposed the underlying crystalline basement which is part of the Arabian-Nubian Shield that formed during Pan-African (Late Proterozoic) orogeny (Greiling et al. 1988). It was represented by Middle to Late Proterozic Metamorphic volcano-sedimentary series, and basic ultrabasic suites, intruded by a wide variety of plutonic rocks, ranging from diorite gabbro to granite, mainly of upper Proterozoic-Paleozoic age and by Cenozoic Alkaline ring complexes.

According to EGSMA, 1992, the geology of the Abu Dabbab area included three principal lithological complexes: the Basic/Ultrabasic Complex, the Volcano-Sedimentary Sequence, and the Intrusive Complex. The Intrusive Complex outcrops in the southern part of the area, constituting a nearly continuous unit with approximately EW and WNW-ESE limits with the Volcano-Sedimentary Sequence.

The basic/ultrabasic assemblage forms several major massifs differently oriented, and a large number of minor scattered bodies characterized by tectonic contacts with the Volcano-Sedimentary Sequence. The ultrabasites are

represented principally by talc-carbonate-serpentine rocks that are considered to be a part of the Pan-African belt (El Sharkawy and El Bayoumi 1979) and interpreted as an ocean floor ophiolite suite tectonically abducted in convergent zones (Shackleton et al. 1980; Ries et al. 1983 and El Gaby et al. 1984, 1988).

Intrusion breccia in the Southern contact of Abu Dabbab apogranite is marked. It consists of angular elongate clasts of altered metasediments (EGSMA, 1992). Fragments display hydrothermal transformation mainly represented by growth of white mica and fluorite. Space among fragments is filled by quartz, feldspar and topaz. Several outcrops of limited size hydrothermal altered rocks were also found, located along the contacts of Abu Dabbab granite with country rocks, which show deeply altered and oxidized rocks, produced probably by hydrothermal alteration on talc-carbonate or volcano-sedimentary rocks.

Fig. 2 shows the simplified geologic map of the Abu Dabbab area and its surroundings, re-plotted after the geologic map 1:100,1000 scale of EGSMA 1991. The map also shows possible surface faults passing through the area

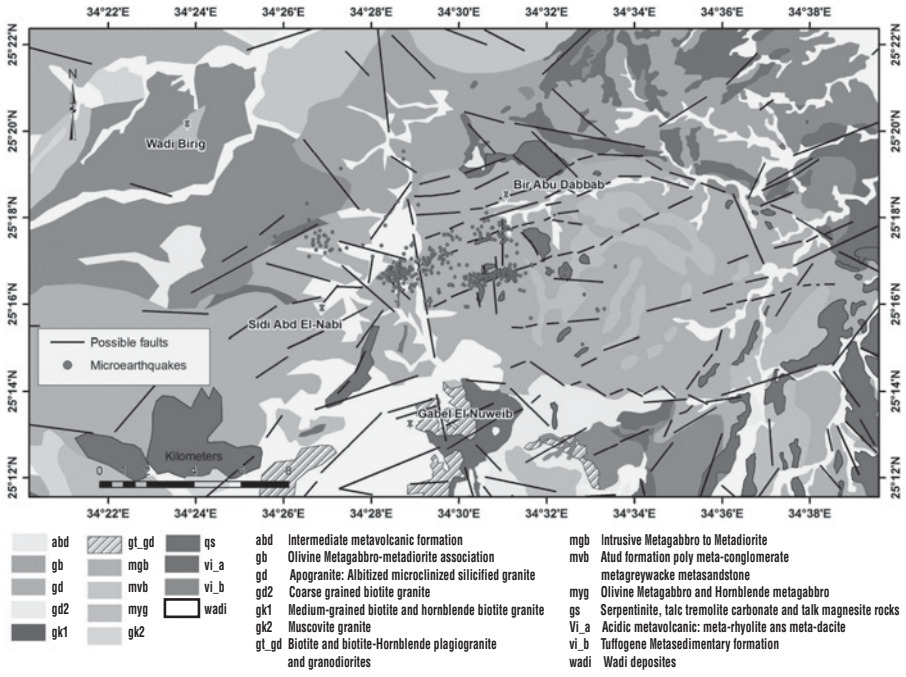

Fig. 2 Simplified geologic map of the Abu Dabbab area and its surroundings, re-plotted after the geologic map 1:100,1000 of EGSMA 1991. The map also shows possible surface faults passing through the area based essentially on the interpretation of 1:40,000 aerial photographs by EGSMA 1992. The microearthquakes are located using the 3D-tomography results of this study.

based essentially on the interpretation of 1:40,000 aerial photographs by EGSMA 1992. Rock unit distribution and foliation trends show a rather complex structural pattern. The interfingering of rocks of the Basic Ultrabasic Complex with rocks of the Volcano Sedimentary Sequence is completely folded and faulted, suggesting that this process belongs to the first deformation phases of the regional tectonic evolution. The EW trending shear zones of the southern sector, affecting also rocks of the Intrusive Complex, belong probably to successive phases of deformation, that may be associated with thrust faulting of the Intrusive Complex plutonites over volcano-sedimentary rocks.

Trend distribution of fault systems (based mainly on a photogeological study) show a rather homogeneous pattern, only with a relative lack of EW faults. NNW to NW faults appear linked to regional foliation trends, while NNE to NE faults generally cut with high angle regional structures. NNE to NE faults belong probably to a younger system.

3 Data selected

More than 850 events are selected for Vp and Vp/Vs inversions, see Fig. 3. The data are the arrival times picked with high precision from digital waveforms with low residuals and good ray coverage from local earthquakes recorded by the Abu Dabbab local telemetered network, operated and maintained by the National Research Institute of Astronomy and Geophysics. This seismic network is equipped with a digital acquisition system and a trigger algorithm for event location and consists of 10 short-period seismometers equipped with a vertical seismometer in addition to one Orion station with three components. Data were sent via telemetry to the acquisition center at Marsa-Alam City.

The selected events are azimuthally well distributed. As can be seen from Fig. 3 all events used in the inversion are concentrated inside the study area. The number of observations for each selected event is not less than 8. The locations were calculated using the HYPO71 program (Lee and Lahr 1975) and once again by the VELEST program. The data set covers the time span from July to August 2004 with local magnitudes ranging from 2 to 3.6 and depths ranging from 3 km to 16 km. Events with high residuals and which are located outside of the invistigated area are excluded from the inversion.

The 3-D Vp inversion was obtained using 8000 P-wave arrival times with an estimated picking accuracy of $\pm$ 0.1s. The data set for the 3-D Vp/Vs model consists of 4000 S-P wave arrival times. The earthquakes for the Vp/Vs models were carefully selected to assure a significant number of S arrival times.

4 The 1-D model

The reliability of the results obtained with the linear tomographic inversion strongly depends on the initial reference model. Kissling et al. (1995) showed

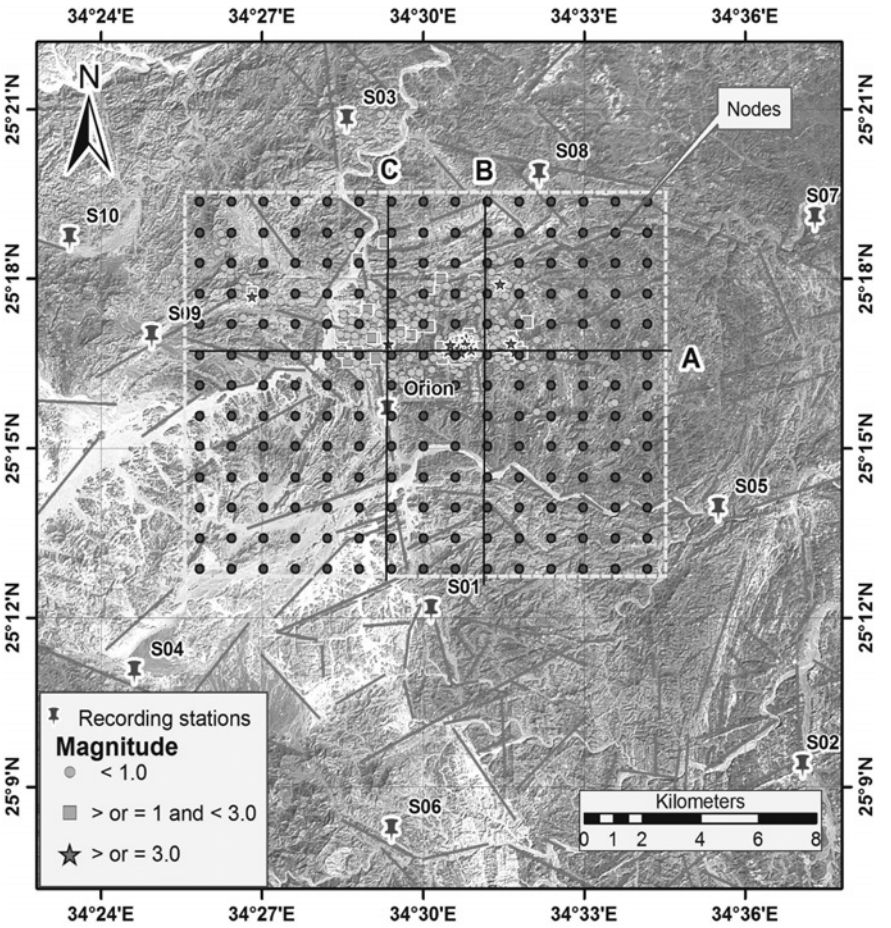

Fig. 3 Location of the 3-D inversion grid nodes superimposed on Landsat^{TM} image. The dashed rectangular box limits the area under investigation. The red lines show possible faults modified after EGSMA 1991 and 1992 and are based essentially on the interpretation of 1:40,000 aerial photographs.

that an inappropriate initial reference could significantly affect the quality of the tomographic results. We therefore followed the Kissling et al. (1995) approach in order to obtain the reference 1-D model of the study area. The 1-D modeling carried out in the current work has been performed with the program VELEST (Kissling et al. 1995) by inverting for hypocenters at every iteration, and by inverting station delays and velocity values every second iteration, until the total RMS value (root mean square misfit of travel time residuals) reduces significantly and stabilizes. The choice of the initial information used as an input model for VELEST was taken from the refraction model of Marzouk (1988).

A comparison between the initial and the inverted (final) 1-D crustal model, as listed in Tables 1 and 2, is shown in Fig. 4. The Vp velocity model is assigned

Table 1 Simplified refraction-based model used as a starting model in the linear inversion.

Depth (km)	Velocity (km/s)
0	3.5
1.5	4.5
3.5	6.0
10	6.6
26	8.0

Table 2 The inverted (final) Vp crustal model for the area, used as a reference model in the 3-D tomography.

Depth (km)	Velocity (km/s)	Depth (km)	Velocity (km/s)
0	4.30	12	6.50
1.0	4. 45	20	6.80
3.0	5.90	25	7.50
6.0	4.30	32	8.10
9.0	6.25		

to the nodes of a 3-D grid and the velocity value at any other point is obtained by linear interpolation between the nodes. The Vp/Vs initial model for the 3-D Vp/Vs inversion, has been calculated for each event by means of the Wadati diagram, (Wadati 1933), Fig. 5a and b, and the average value is 1.71. This mean value is calculated using 220 microevents having at least four S-P times, correlation coeffcient R = 0.9 for each Vp/Vs value and RMS less than 0.05.

5 Inversion method and procedure

The calculation of the 3-D velocity structures was carried out using the SIMUL2000 routine (Thurber et al. 1999). The algorithm produces 3-D Vp, 3-D Vp/Vs, and also 3-D Vs crustal structural models using P-wave and S-P travel times from local earthquakes and explosions. It was originally developed by Thurber (1983), but experienced many subsequent modifications (e.g., Um and Thurber 1987; Eberhart-Phillips and Michael 1993; Rietbrocke 1996; Thurber et al. 1999). The structural model is defined on nodes at the intersections of a possibly unevenly spaced rectangular grid, and the model parameters between neighboring grid nodes are determined by linear B-spline interpolation.

The area under investigation is represented digitally by grids and a map view of the model is shown in Fig. 2. The model dimensions are 15 km in the X-direction, 13 km in the Y direction, and 15 km in the Z-direction (depth). The grid extends: in the X-directions at -7, -6, -5, -4, -3, -2, -1, 0, 1, 2, 3, 4, 5, 6, and 7 km; in the Y-directions at 4, 3, 2, 1, 0, -1, -2, -3, -4, -5, -6, -7, and -8 km;

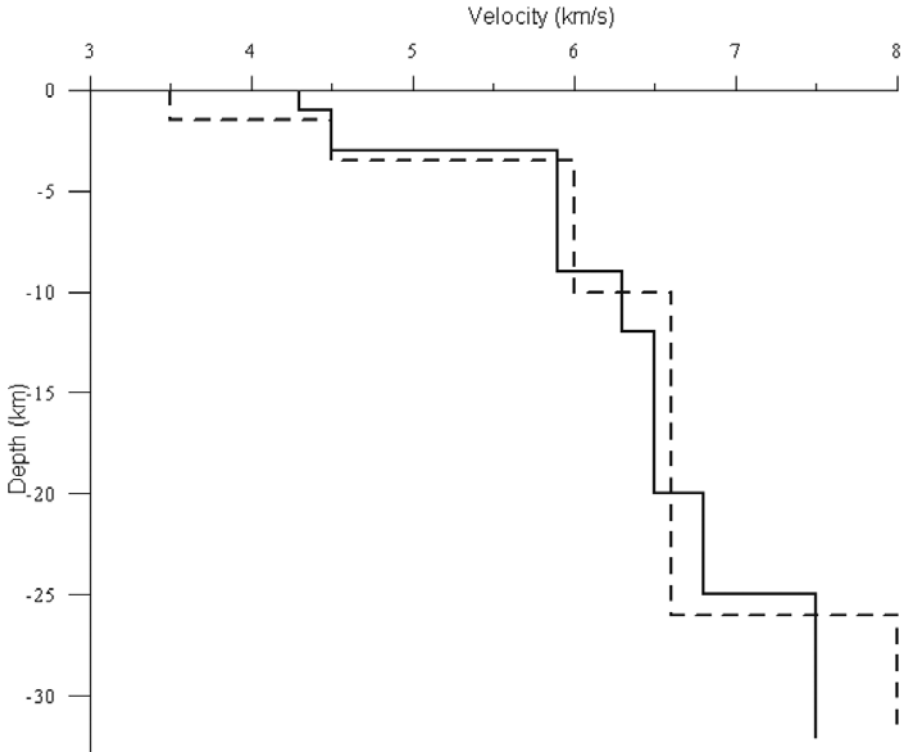

Fig. 4 Comparison between the derived 1-D reference model (solid line) and the starting model (dashed line).

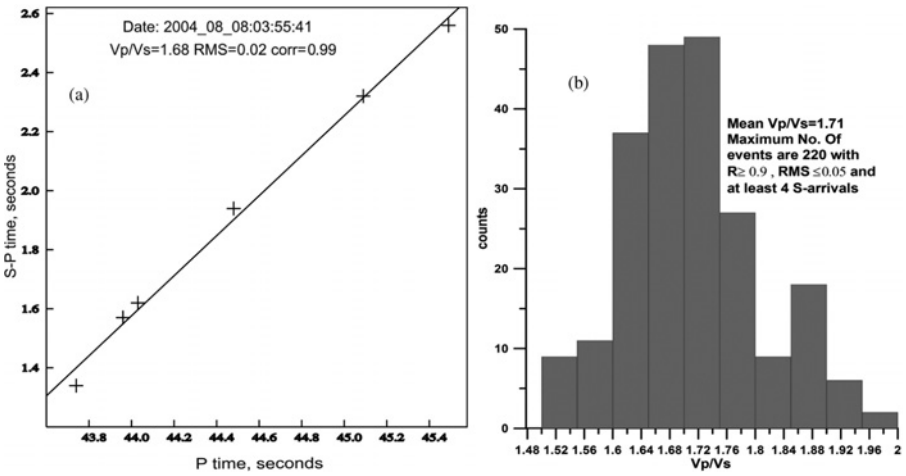

Fig. 5 (a) Wadati diagram example of the event 8.8.2004 at 03h 55m 41s. From the slope, the vp/vs value is 1.68 with error 0.02. (b) Histogram of Vp/Vs values used for the determination of the mean Vp/Vs value.

in Z-directions at 0, 1.0, 3.0, 4, 5, 6, 7, 8, 10, 12, and 15 km. The coordinates of the grid center are latitude 25°17′20″N and longitude 34°30′00″E.

The calculation starts by assigning the velocity values of the 1-D reference model (Table 2) to all the nodes of the 3-D grid. The travel time from the hypocenter to the station is calculated by the pseudo-bending method (Um and Thurber, 1987). The solution is then obtained by an iterative procedure, solving for hypocenter location and calculating the velocity of the medium, with a damped least-squares approach. The next stage is the proper choice of the damping parameter.

The damping parameter for each inversion is chosen empirically by evaluating a trade-off curve of data variance and solution variance, thus the damping will vary with the model grid and the data set (Eberhart-Philips 1986). The best selected damping values for the Vp velocity model and Vp/Vs model are 5 and 10, respectively, as shown in Fig. 6. These values lead to a significant reduction in the data variance with only a moderate increase in model roughness.

In the present study, the following steps are followed to calculate the 3-D Vp and Vp/Vs models. During the first steps of tomographic inversion for 3-D Vp and Vp/Vs, an inversion step, with only one iteration, has been done to test the configuration of the model grid. This configuration is tested by observing the "derivative weight sum" (DWS, number of rays per each node) result. The goal of this step is to investigate the adequacy of the ray coverage and the resolution, see Fig. 7. The 3-D Vp and Vp/Vs models are calculated by fixing the damping values for Vp and Vp/Vs, respectively, as obtained from the damping parameters test and allowing hypocenter relocation. The final 3-D Vp and Vp/Vs models were obtained after five iterations. The topography of the study area, taking into the station elevation and the station corrections account, has been considered in the inversion process.

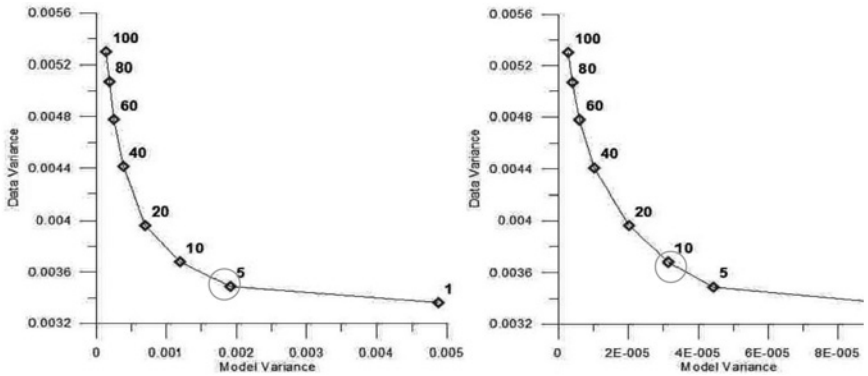

Fig. 6 Trade-off curve for the variance of the velocity perturbations and root mean square travel time residuals. Numbers near the blue diamonds denote the damping parameters adopted for the inversions. Circled values 5 and 10 are selected as the best damping value for Vp and Vp/Vs models, respectively.

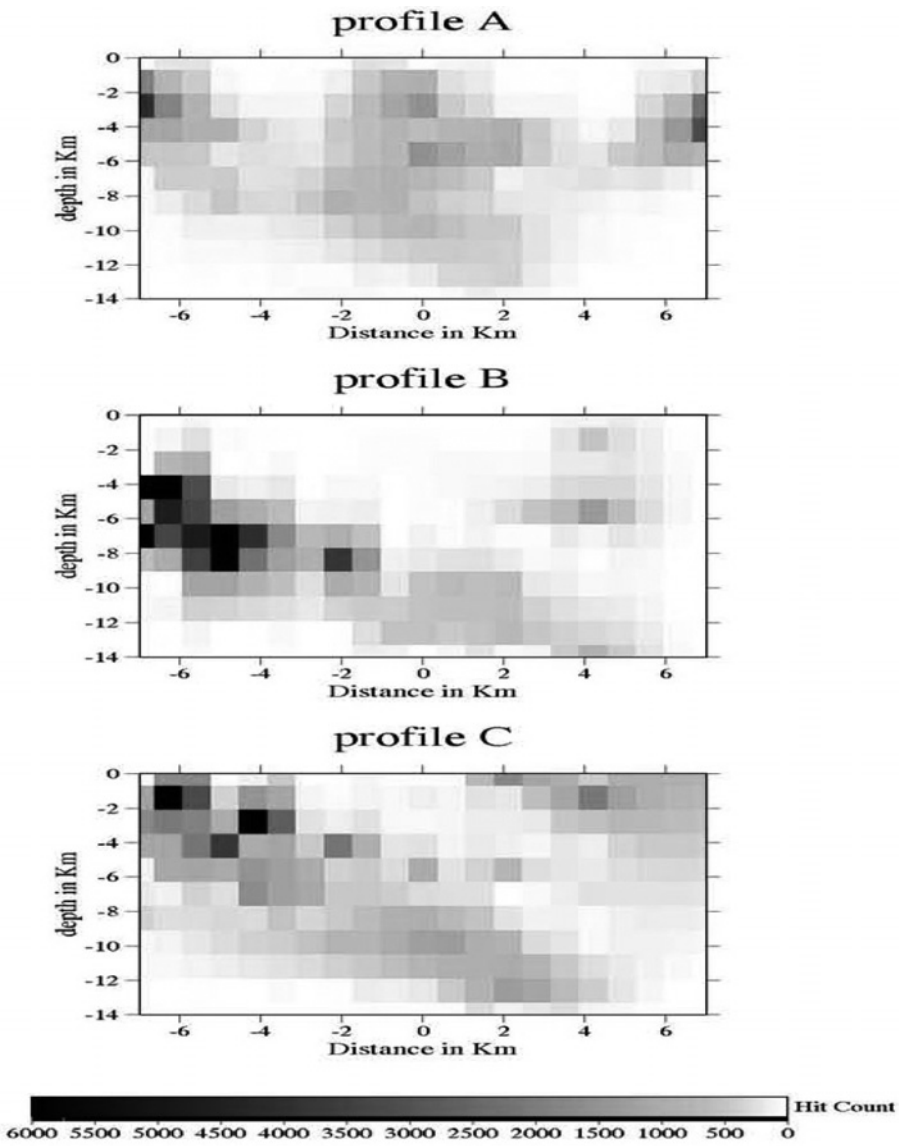

Fig. 7 Distribution of the number of rays passing through each grid node (hit counts). Hit counts are represented for each profile, A, B, and C. The hit count scale is shown at the bottom.

6 Discussion and conclusion

The best measure to estimate the quality of the inversion result is given by the resolution matrix. The resolution matrix describes the distribution of the information for each node, such that each row is the averaging vector for a parameter. In this study most of the earthquake hypocenters are in the depth range

from 4 to 15 km, and the 3-D Vp, Vp/Vs and Vs models are resolved. To minimize numerical artifacts, damping allows only small velocity perturbations in areas of low resolution.

Based on the 3-D Vp and Vp/Vs models, we relocated more than 850 events that occurred within the study area during the period 1-20 August 2004 in order to give an improved representation of the seismicity pattern to be compared with the calculated tomographic model. Through tomographic results, the velocity cross sections that are constructed for Vp, Vs, and Vp/Vs are represented in Figs. 8, 9, and 10, respectively, through profiles A, B, and C. From these sections we noted that the distributions of Vp and Vp/Vs are characterized by marked lateral and depth variations, suggesting the presence of significant structural heterogeneities. If these velocity contrasts and variations are the expression of horizontal and vertical discontinuities, an attempt to delineate the fault geometry at depth is natural (Eberhart-Philips and Michael 1993).

The overall Vp and Vp/Vs pattern reflects the complex geologic features of the study area. The mean value of Vp/Vs is a very important parameter to infer some rheological features and to understand the spatial distributions of earthquakes. The low Vp/Vs areas may indicate higher rigidity crustal rocks with brittle behavior, while the increase of Vp/Vs ratio may identify areas of relatively more soft crustal rocks with ductile behavior (Seiduzova et al. 1985).

Low P-wave velocity anomalies can be seen through different depths and they could be related to the intersection among the faults cutting the area. The high P-wave velocity anomalies (brittle rocks) are bounded by low velocity anomalies that correspond to more ductile rocks. In fact the low Vp and high Vp/Vs anomalies could be due to some magma intrusions present at depth. These high Vp/Vs anomalies could suggest the occurrence of small size volumes of hot intrusive igneous rocks initiated at different depths. The origin of these intrusive igneous rocks could be explained by the presence of fractional heating at depth that could arise from the reactivation of old shear zones during the formation of active Red Sea rift.

Boulus et al. (1990) and Morgan et al. 1985 studied the Red Sea coastal thermal anomaly in Egypt and they perceived for the Abu Dabbab area a high heat flow value of about 92 $mW/m^2 \pm 10$, which is more than twice the average value of Egyptian Eastern desert (47 mW/m^2). El Hady (1993), reported, from the distribution of earthquake focal depths and rheological studies, that the brittle-ductile transition in the Abu Dabbab area occurs at a relatively shallow depth range ($9 \sim 10$ km) which is consistent with the measured heat flow value of the Abu Dabbab area.

Using the 3-D velocity model for the relocation of the same events that have been used in the structure inversion, shown in the velocity sections A, B, and C, the earthquakes are strongly clustered in correspondence with the central high velocity anomaly and are concentrated at high and low velocity contrasts. Such clustering can be explained by the focusing of both local and regional stress in this zone of strong rigidity contrast.

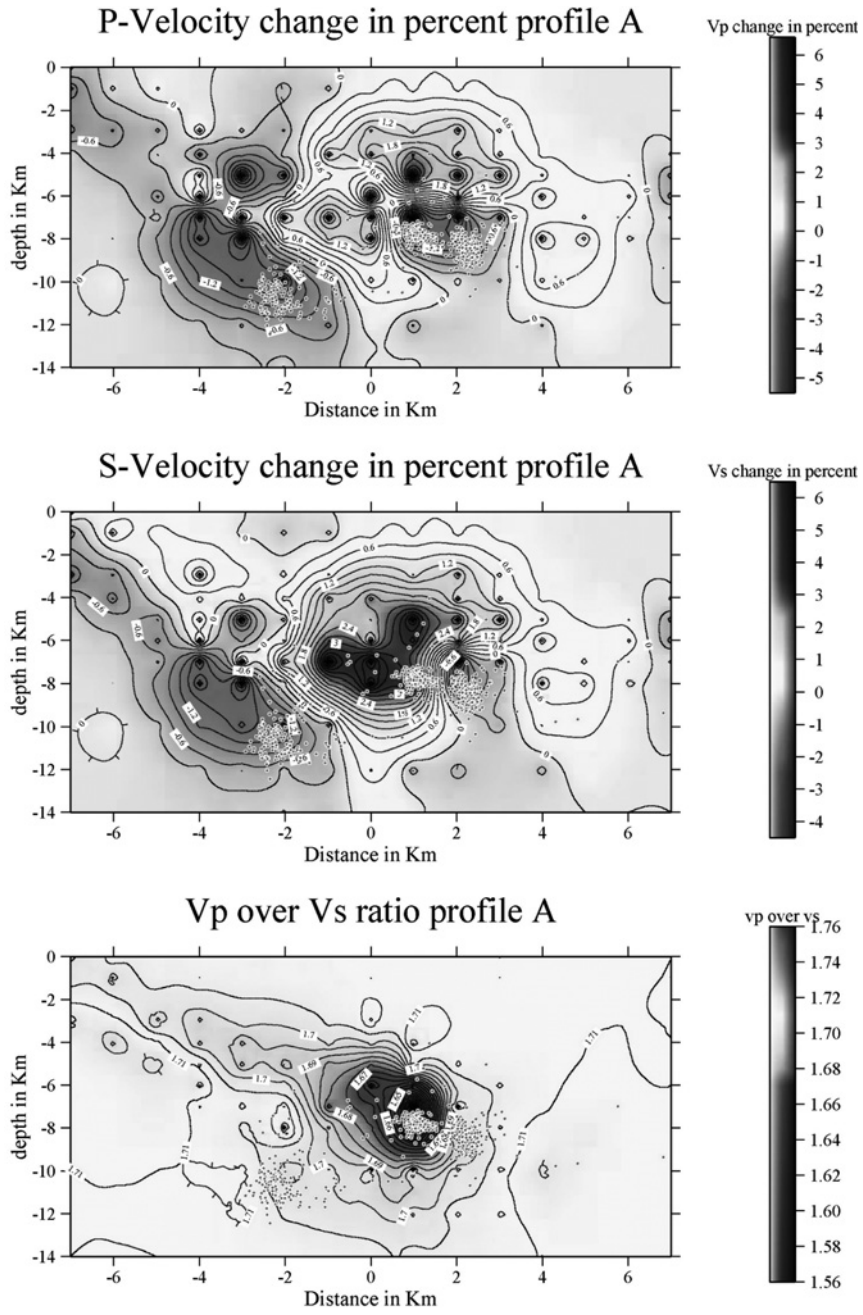

Fig. 8 Profile A, vertical cross-section, of Vp, Vs and Vp/Vs variations and relocated hypocenters. Red and blue colors denote low and high Vp and Vs velocities, respectively, while blue and red colors denote low and high Vp/Vs ratio, respectively. Small open circles show the relocated earthquakes which occurred within a 3 km wide band around each profile. The percent velocity perturbation scale is shown at the right of each cross section.

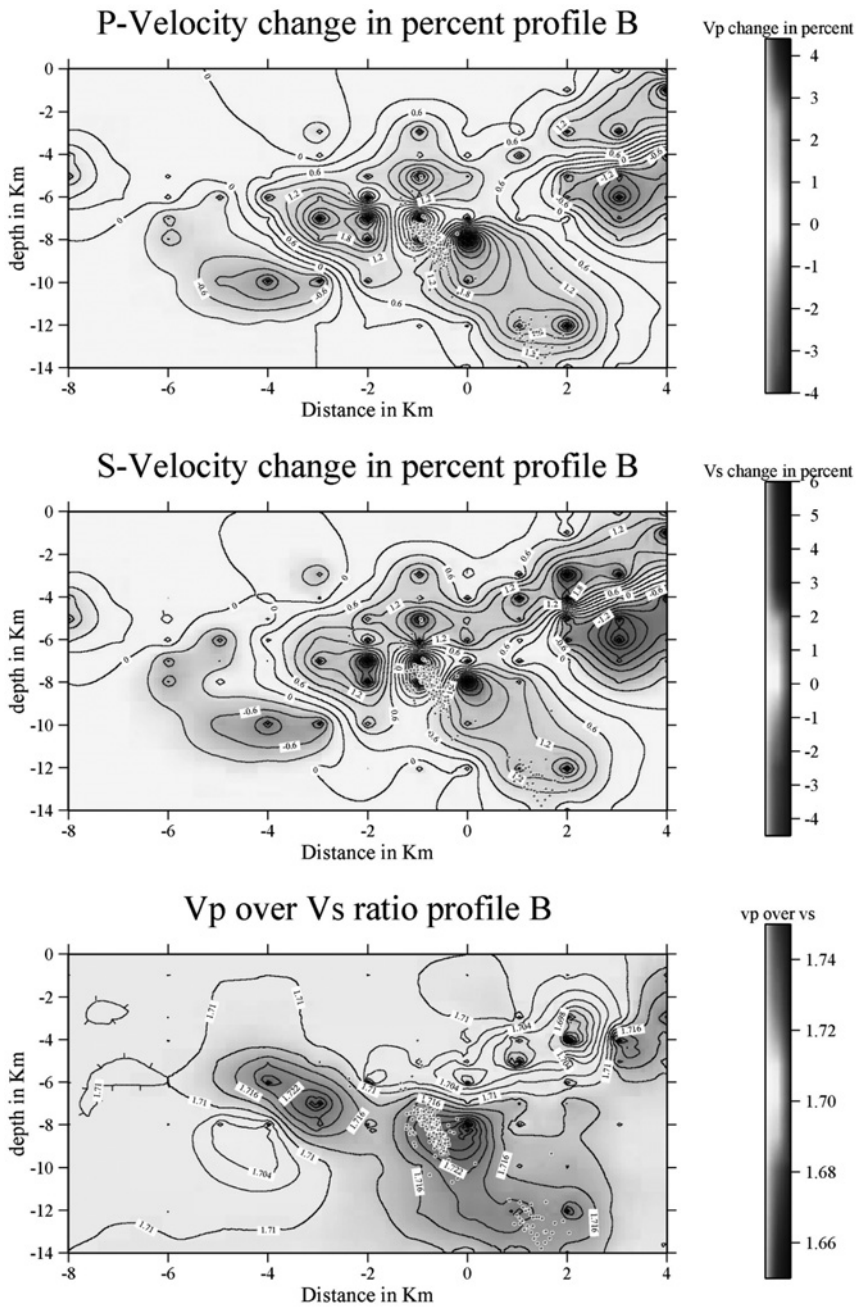

Fig. 9 Profile B, vertical cross-section, of Vp, Vs and Vp/Vs variations and relocated hypocenters. Red and blue colors denote low and high Vp and Vs velocities, respectively, while blue and red colors denote low and high Vp/Vs ratio, respectively. Small open circles show the relocated earthquakes which occurred within a 3 km wide band around each profile. The percent velocity perturbation scale is shown at the right of each cross section.

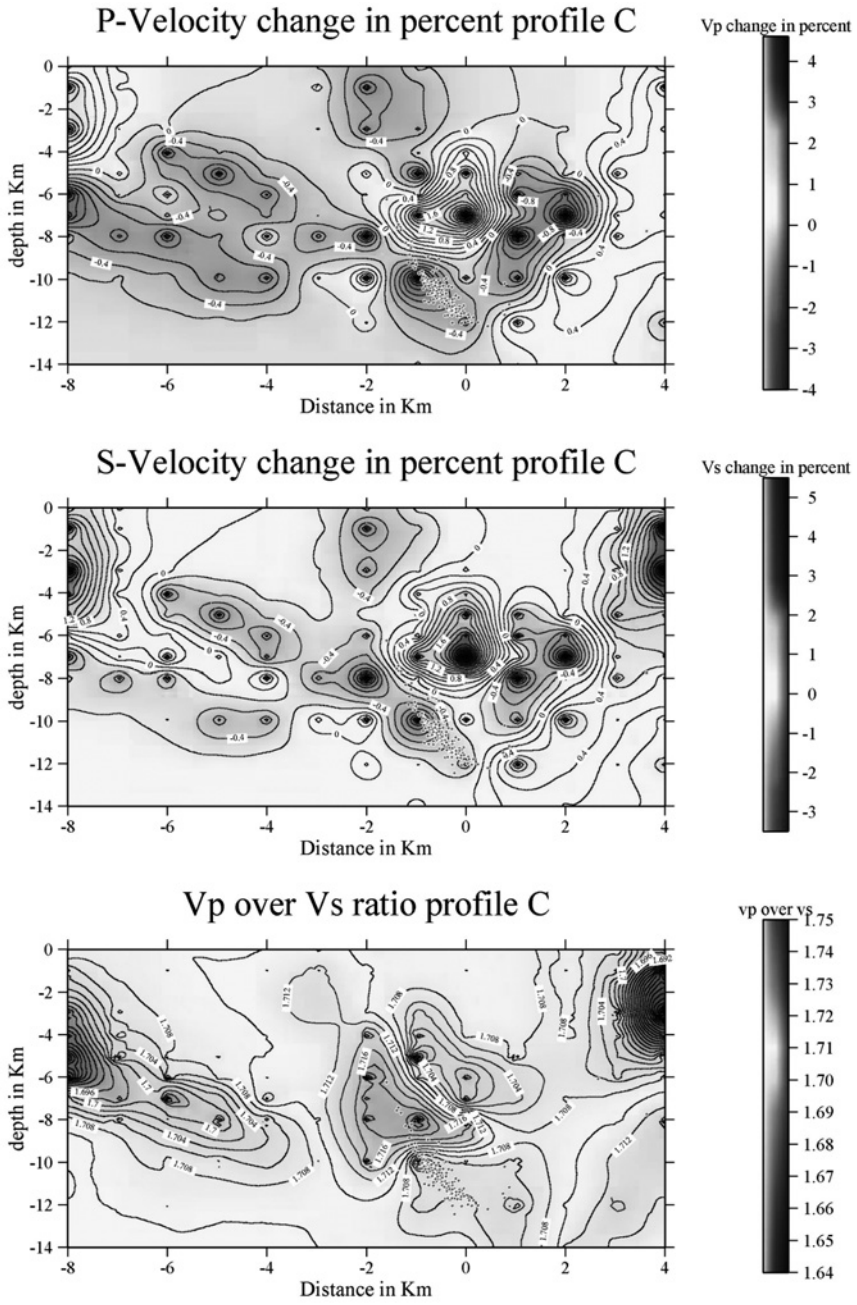

Fig. 10 Profile C, vertical cross-section, of Vp, Vs and Vp/Vs variations and relocated hypocenters. Red and blue colors denote low and high Vp and Vs velocities, respectively, while blue and red colors denote low and high Vp/Vs ratio, respectively. Small open circles show the relocated earthquakes which occurred within a 3 km wide band around each profile. The percent velocity perturbation scale is shown at the right of each cross section.

Hydrothermal alteration on talc-carbonate and serpentine rocks or volcano-sedimentary rocks have been noticed in the study area (as seen before in the geologic setting section). Hydrated mineral assemblages generally have substantially lower seismic velocities than their parent rocks; this effect is well known for serpentinite. The seismic velocity and density of the mantle decrease while Vp/Vs increases with the increasing degree of serpentinization in crustal rocks.

Serpentinization may generate seismic reflectivity, an increase in magnetization, an increase in electrical conductivity, and a reduction in mechanical strength.

After seismicity relocations, using the new 3-D model, most of the seismic events occur as clusters. The majority of these clusters are located in the depth ranges, from 5 to 8 km and from 8 to 12 km. The earthquake swarms recorded during the past century and the currently located seismicity have focal depths not greater than 12 km. This may be taken as an indication that ductile material, at high pressure and temperature, or fluid, is present below the high rigidity material in the upper crust, supporting the presence of intrusive igneous rocks through the upper crust of the Abu Dabbab area.

As a test of reliability and accuracy of the new 3-D model in the location of events, we used this new model for the relocation of 400 selected events, evenly distributed in the study area, that were not used in the structure inversion. Comparing the locations of these events, obtained using the old model (Fig. 10a) and the new model (Fig. 10b), we observe that the epicenter's distribution is more clustered and concentrated at the intersections among the faults cutting the area, when the new model is used. On the other hand, by using the old model, the seismicity locations are scattered and widely distributed over the area considered. Therefore, the improvement noticed in the correlation between relocated events and the existing faults in the Abu Dabbab area is a real achievement due to the availability of the new 3-D model.

The appearance of most of the seismicity clustered around these intersections supports and is in agreement with the hypothesis of the intersection theory by Talwani and Rajendran (1991). A model proposed by Gabrielov et al. (1996) implies that block interaction along intersecting faults leads to stress and strain accumulation and secondary faulting around the intersection. This causes the generation of new faults of progressively smaller size, so that a mosaic structure, a node, is formed around the intersection. The instability of fault junctions was also studied by McKenzie and Morgan (1969), King (1983, 1986), Cronin (1992), and McCaffrey et al. (2000).

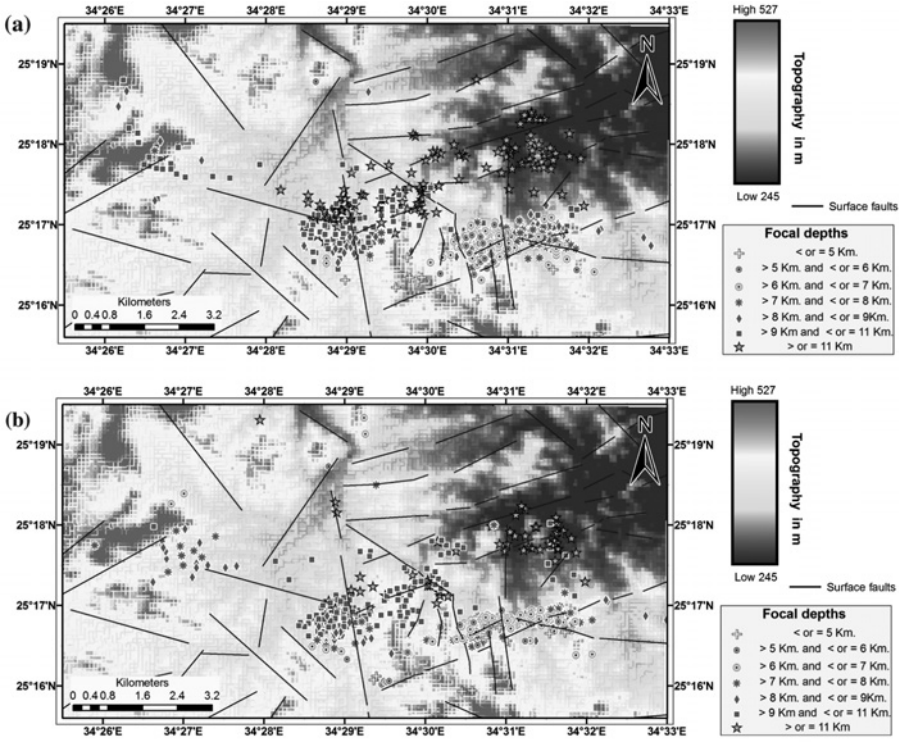

Fig. 11 Topographic map with the location of the earthquakes which were not used in the inversion, (a) locations using the old model, and (b) locations using the new model. Three ellipses define the three zones occupied by the relocated epicenters. Solid lines indicate the possible faults (see, Fig. 2 for reference). Different focal depths are indicated with different symbols.

Acknowledgements. We are grateful for the kind assistance and support from the Office of External Activities OEA, ICTP, Trieste, Italy and also for the kind help of our colleagues at DST, University of Trieste, Italy.

We would also like to express our appreciation to our colleagues at the Seismolgy Department, Egyptian National Seismological Network ENSN who worked hard in establishing the mobile arrays Network around the study area for the collection of data.

References

1. Aki K, Lee WHK (1976) Determination of Three-dimensional velocity anomalies under a seismic array using first P arrival times from local earthquakes. 1. A homogeneous initial model: J Geophys Res 81: 4381–4399
2. Badawy A, El-Hady Sh, Abdel-Fattah AK (2008) Microearthquakes and neotectonics of Abu-Dabbab, eastern desert of Egypt. Seismological Research Letters 79(1): 55–67
3. Boulos FK, Morgan P, Hennin SH, El-Sayed AA, Melik YS (1990) The tectonic structure of northern Africa from Gravity data, personal communication

4. Cronin VS (1992) Types and kinematic stability of triple junctions. Tectonophysics 207: 287–301
5. Daggett PH, Morgan P (1977) Egypt and the northern Red Sea: New microearthquake data. Trans Am Geophys Union. 58: 1198
6. Daggett PH, Morgan P, Boulos FK, Hennin SF, El-Sherif AA, El-Sayed AA, Basta NZ, Melek YS (1986) Seismicity and active tectonics of the Egyptian Red Sea margin and the northern Red Sea. Tectonophysics 125: 313–324
7. Eberhart-Philips D (1986) Three-dimensional velocity structure in Northern California Coast Ranges from inversion of Local earthquake arrival times. B.S.S.A. 76: 1025–1052
8. Eberhart-Philips D, Michael AJ (1993) Three-dimensional velocity structure, seismicity and fault structure in the Parkfield region, central California. Geophys Res 98: 737–758
9. El Gaby S, El-Nady O, Khudeir AA (1984) Tectonic evolution of the basement complex in the Central Eastern Desert of Egypt. Geological Rundschau 73: 1019–1036
10. El Gaby S, List FK, Tehrani R (1988) Geology, evolution and metallogenesis of the Pan-African Belt in Egypt. In: El Gaby S, Greiling R. (eds.): The Pan-African Belt of Northeast Africa and Adjacent Areas: Tectonic Evolution and Economic Aspects. Freidr. Vieweg&Sohn, Braunschweig/Wiesbaden: 17–68
11. EGSMA (1991) Geological maps of Marsa Alam and Umm Gheig 1:100,1000 scale. The Egyptian Geologic Survey and Mining Authority
12. EGSMA (1992) Abu Dabbab Deposits, internal report. The Egyptian Geologic Survey and Mining Authority. Vol. 1, p. 156
13. El-Hady ShM (1993) Geothermal evolution of the Red Sea margin and its relation to earthquake activity. MSc Thesis. Cairo University, Cairo, Egypt
14. El Sharkawy MA, El Bayoumi, RM (1979) The ophiolites of Wadi Ghadir area, Eastern Desert, Egypt. Annals of the Geological Survey of Egypt 9: 125–135
15. Fairhead JD, Girdler RW (1970) The seismicity of the Red Sea, Gulf of Aden and Afar triangle. Phil Trans R Soc A 267: 49–74
16. Gabrielov A, Keilis-Borok V, David DJ (1996) Geometric incompatibility in a fault system. PNAS 39(9): 3838–3842
17. Greiling RO, Kroner A, ElRamly MF, Rashwan AA, (1988) Structural relations between the southern and central parts of the Eastern Desert of Egypt: details of fold and thrusts belt. In: El Gaby S, Greiling R (eds.): The Pan-African Belt of the NE Africa and Adjacent Areas. Tectonic Evolution and Economic Aspects. Freidr. Vieweg&Sohn, Braunschweig/Wiesbaden: 121–145
18. Hassoup A (1987) Microearthquakes and magnitude studies on earthquake activity at Abu Dabbab region, Eastern Desert Egypt. " Thesis M.Sc., Fac Sci, Cairo Univ. pp. 1–169
19. Hamada K (1968) Ultra micro-earthquakes in the area around Matsushiro, Bull Earthq Res Inst 46: 271–318
20. Ibrahim ME, Yokoyama I (1994) Probable origin of the Abu Dabbab earthquakes swarms in the Eastern Desert of Egypt. Bull IISEE 32 (1998)
21. Kebeasy RM (1990) Seismicity. In: Said R (ed.): Geology of Egypt. Balkema, Rotterdam: 51–59
22. King G (1983) The accommodation of large strains in the upper lithosphere of the Earth and other solids by self-similar fault systems: The geometrical origin of *b*-value. Pure Appl Geophys 121: 761–815
23. King G (1986) Speculations on the geometry of the initiation an termination processes of earthquake rupture and its relation to morphology and geological structure. Pure Appl Geophys 124: 567–583
24. Kissling E, Solarino S, Cattaneo M (1995) Improved seismic velocity reference model from local earthquake data in Northern Italy. Terra Nova 7: 528–534

25. Lee WHK, Lahr JC (1975) A computer Program for determining hypocenter, magnitude, and first motion pattern of local earthquakes. U.S. Geol Survey open file Rep: 75–311
26. Martinez F, Cochran JR (1988) Structure and tectonics of the northern Red Sea: catching a continental margin between rifting and drifting. Tectonophysics 150: 1–32
27. Marzouk I (1988) Study of the crustal structure of Egypt deduced from deepseismic and gravity data. Ph D Thesis Hamburg Univ. Hamburg
28. McCaffrey R, Long MD, Goldfinger C., Zwick P, Nabelek J, Smith C (2000) Rotation and plate locking at the southern Cascadia subduction zone. Geophysical Research Letters 27: 3117–3120
29. McKenzie, DP, Morgan WJ (1969) The evolution of triple junctions. Nature 224: 125–133
30. Morgan P, Keller GR, Boulos FK (1981) Earthquake cannons in the Egyptian Eastern Desert. Bull Seismol Soc Am 71: 551–554
31. Morgan P, Boulos FK, Hennin SF, El-Sherif AA, El Syed AA, Basta NZ, Melek YS (1985) Heat flow in eastern Egypt: the thermal signature of continental break up. J Geodyn 4: 107–131
32. Rietbrock A (1996) Entwicklung eines Programmsystems zur konsistenten Auswertung großer seismologischer Datensätze mit Anwendung auf die Untersuchung der Absorptionsstruktur der Loma-Prieta-Region. Kalifornien, PhD Thesis, LMU München
33. Seiduzova SS, Surov VP, Matasova lM, Atabev KA, Suchkova SS, Riabova SD, Yankovaskaya NN (1985) Special features of deep structures of earth's crust and seismic hazard for the territory of eastern Uzbekistan. Paper presented at the 3rd international symposium on the analysis of seismicity and seismic risk. Liblice, Czechoslovakia, June: 17–22
34. Shackleton RM, Ries AC, Graham RH, Fitches WR (1980) Late Precambrian ophiolitic mélange in the Eastern Desert of Egypt. Natur 285: 472–474
35. Talwani P, Rajendran K. (1991) Some seismological and geometric features of intraplate earthquakes. Tectonophys 186: 19–41
36. Thurber C (1983) Earthquake locations and three-dimensional crustal structure in the Coyote Lake area, central California. PhD Thesis, Mass. Inst. of Tecnol., Cambridge
37. Thurber CH, Eberhart PD, Evans JR (1999) Local earthquake tomography: velocity and Vp/Vs-theory, seismic tomography. In: Iyer HM, Hirahara K (eds.): Theory and practice. Chapman and Hall, London: 563–583
38. Um J, Thurber C (1987) A fast algorithm for three-dimensional seismic ray tracing (abst.). Eos Trans AGU 67: 304
39. Wadati A (1933) On travel time of earthquake waves. Part II. Geophys Mag 7: 101–111
40. Zhao D, Laske G (2005) P-wave tomography and origin of the Ghangbai intraplate volcano in Northeast Asia, Techtonophysics 397: 281–295